ENVIRONMENTAL RESEARCH
LETTERS



LETTER • OPEN ACCESS

# North American cold events following sudden stratospheric warming in the presence of low Barents-Kara Sea sea ice

To cite this article: Pengfei Zhang *et al* 2020 *Environ. Res. Lett.* **15** 124017

Environmental Research Letters

LETTER

# North American cold events following sudden stratospheric warming in the presence of low Barents-Kara Sea sea ice

**Pengfei Zhang**[1,2], **Yutian Wu**[3], **Gang Chen**[1] and **Yueyue Yu**[4]

[1] Department of Atmospheric and Oceanic Sciences, University of California, Los Angeles, CA 90095, United States of America
[2] Department of Meteorology and Atmospheric Science, Pennsylvania State University, University Park, PA 16802, United States of America
[3] Lamont-Doherty Earth Observatory, Columbia University, Palisades, NY 10964, United States of America
[4] School of Atmospheric Sciences, Nanjing University of Information Science & Technology, Nanjing, People's Republic of China

**E-mail:** pfz5053@psu.edu, zpengfei@atmos.ucla.edu and gchenpu@atmos.ucla.edu

**Keywords:** sudden stratospheric warming, Barents-Kara Sea sea ice, North American cold events

Supplementary material for this article is available online

OPEN ACCESS

RECEIVED
31 July 2020

REVISED
24 September 2020

ACCEPTED FOR PUBLICATION
16 October 2020

PUBLISHED
27 November 2020



## Abstract

While the relationship between the Arctic sea ice loss and midlatitude winter climate has been well discussed, especially on the seasonal mean scale, it remains unclear whether the Arctic sea ice condition affects the predictability of North American cold weather on the subseasonal time scale. Here we find that, in the presence of low Barents-Kara Sea (BKS) sea ice, sudden stratospheric warmings (SSWs) can favor surface cold spells over North America at the subseasonal timescale based on observations and model experiments. A persistent ridge of wave-2 pattern emerges over the Bering Sea-Gulf of Alaska several weeks after the SSW onset, with a coherent structure from the stratosphere to the surface, which, in turn, is conducive to synoptic cold air outbreaks in Canada and midwestern USA. This highlights a planetary wave pathway relating to BKS sea ice changes, by which the stratospheric polar vortex impacts the regional surface temperature on the subseasonal scale. In contrast, this mechanism does not occur with positive BKS sea ice anomaly. These findings help to improve the subseasonal predictability over North America, especially under the background of rapid change of Arctic sea ice in a warming world.

## 1. Introduction

Despite several unusually cold winters over the Northern Hemisphere midlatitude continents in recent years, it remains unclear how and to what extent the cold events were caused by anthropogenic climate change or internal variability [1, 2]. Some studies have claimed a connection between the rapid Arctic warming/sea ice loss and the occurrence of cold winters over Eurasia and North America in recent decades [3–7], but these analyses are also challenged by others using different diagnostic methods, observational datasets and numerical model experiments [8–12]. While the debate on the impact of Arctic warming/sea ice loss in the observed cold winters is far from resolved [13, 14], some recent studies suggested the role of the sea ice condition in improving the subseasonal forecast [15, 16].

Sudden stratospheric warmings (SSWs) are abrupt decelerations and reversals of the zonal wind in the winter stratosphere due to upward wave propagation from the troposphere and resulting wave breaking in the stratosphere [17]. They are known to affect the tropospheric circulation and surface temperature via downward influence. SSWs are typically followed by the negative phase of Arctic Oscillation (AO) in the troposphere, with a surface high pressure anomaly centered near Greenland and a cold anomaly over northern Eurasia [18–21]. An interesting phenomenon is that some years with SSWs, regardless of a displacement or splitting of the polar vortex (see the discussion later), were among the years of cold air outbreaks over North America [22, 23]. The coldest and snowiest extreme on record in the midwestern U.S.A and eastern Canada in late January 2019 was preceded by an SSW (the 2019 cold event hereafter), which caused enormous economic losses and casualties [24]. Although operational models show a good prediction skill for the timing and structure of polar vortex breakdown beyond 1–2 weeks, the skill is

highly dependent on the model performance in simulating the stratospheric dynamics, data assimilation and initial conditions [25–28]. It has been found that sea ice conditions, especially those over the Barents-Kara Sea (BKS), as one of the boundary conditions that can significantly perturb the stratospheric circulation and the two-way stratosphere-troposphere coupling [29–31]. However, it remains unknown whether and how the surface impact of SSWs could be affected by the Arctic sea ice conditions.

In this letter, we provide both observational and modeling evidence that North American cold events are found about a month after the SSW events in the presence of lower BKS sea ice, while they are absent given a positive BKS sea ice anomaly. We further demonstrate that lower BKS sea ice conditions affect the pattern of the stratospheric circulation during SSWs, which further influences the surface temperature over North America via downward influence at the sub-seasonal timescale.

## 2. Materials and methods

### 2.1. Data analysis

The ERA-Interim reanalysis on a resolution of 1.5° × 1.5° grid in 1979–2019 is used [32]. The sea ice concentration (SIC) is 25 km × 25 km passive microwave satellite observation, Nimbus-7 SMMR and DMSP SSM/I-SSMIS, with the NASA team algorithm Version 1 from NSIDC [33]. We define the late autumn BKS SIC index using the sea ice area in the region of 15°–100°E and 70°–82°N during November (figure S1) (available online at https://stacks.iop.org/ERL/15/124017/mmedia. The reason that we focus on the BKS region is that the sea ice variability and associated warming over this area is more effective in influencing the stratosphere-troposphere coupling than other regions over the Arctic [3, 34]. SSW in this study is simply defined as the reversal of 60°–90°N zonal mean zonal wind at 10 hPa during November to March [35]. A discussion of the choice of the SSW definition can be seen in Supplementary Material (SM). The 1st day with zonal wind reversal is identified as the central day (day 0) listed in table S1. 34 SSWs are identified in 1980–2019 for composite analysis. Since the SSW sample size is limited in observations, all SSW cases are simply divided into two groups conditioned on the BKS SIC index lower and greater than 0 (17vs17), referred to as LoSIC and HiSIC respectively. The departure from the corresponding (HiSIC or LoSIC) daily climatology is extracted for analysis, but the results are insensitive to the choice of climatology and similar results are found with 1980–2019 climatology (not shown). The correlation coefficient between BKS SIC index and Nino3.4 index is small and not significant, indicating the results in this study are insensitive to ENSO. In addition, since this study focuses on the current climate, the grouping of low and high SIC winters is on the basis of current climatology defined by WMO, i.e. mean of 1981–2010. Similar conclusions are found with 2–9 year bandpass filtered observations (with emphasis on the interannual variability) and with the first 30 years only (figures S1 and S2).

### 2.2. Model experiments

A stratosphere-resolving atmospheric circulation model, SC-WACCM4, the atmosphere component of CESM 1.2, with specified chemistry rather than the full interactive chemistry version WACCM4, is used [36]. The removal of interactive chemistry much reduces the computational cost without changing the climatology and variability of the atmospheric circulation in the stratosphere and troposphere, which makes SC-WACCM4 suitable for studies of stratosphere-troposphere dynamical coupling [36]. The simulated frequency of SSWs is about 0.66 per winter and is, therefore close to the observed value of 0.84 (figure S9). The model has 1.9° × 2.5° horizontal resolution and 66 vertical levels with the model lid at 140 km.

In experiments, SST and SIC from the coupled simulations with CESM1-WACCM4 for CMIP5 are prescribed as the model's surface boundary condition. In the control run (hereafter referred to as Ctrl), the repeating climatological seasonal cycle of SST and SIC, from the historical simulations (average of 7 ensembles) and averaged during 1980–1999, is prescribed. In the perturbation run, referred to as BKSIC, the settings are identical to that of the Ctrl but the SIC in the BKS region is replaced by that in the CMIP5 RCP8.5 outputs (average of four ensembles) averaged during 2080–2099. The SST in the BKS region is also replaced with RCP8.5 SST in the open water areas that used to be covered by sea ice in Ctrl run. Although the projected sea ice changes were used in this study, the autumn sea ice difference between the Ctrl and the BKSIC run (−20%) is comparable to the forcing magnitude (−18%) obtained from HadISST in [37] (see supplementary discussion in [30]) due to the underestimation of sea ice changes in climate models [38, 39]. The Ctrl run is regarded as the higher sea ice condition compared to the BKSIC run. There are two sets of 274 winters and 181/217 SSWs in Ctrl and BKSIC runs for analysis, respectively. Details of experiments and supplementary nudging experiments to support the conclusions can be seen in SM.

### 2.3. Diagnostics and statistical methods

Statistical significance is assessed by using 10 000 times bootstrap resampling with replacement. The same method is employed to calculate the confidence interval in figure S9. The two-tailed two-sample Kolmogorov–Smirnov (KS) test is used to compare the probability density function (PDF) of surface air temperature anomaly (SATa) following SSW to that of the whole winters in figure 3. The null hypothesis,

that the distributions of two samples are the same, is rejected when $P \leq 0.01$. Two-dimensional kernel density estimate is employed to explore the distribution changes of the bivariate density of North American cold status and stratospheric ridge anomaly in figure 5. The 2-D density estimate is based on 10 000 times bootstrap resampling with replacement for the mean of 17/17 samples (the sample sizes in LoSIC/HiSIC) from the simulated 217/181 events in BKSIC/Ctrl runs. We also compare the distributions in each dimension using KS test. Wave activity flux (WAF) is employed to diagnose the wave propagation anomalies in section 4.2 (see details in SM).

## 3. Results

### 3.1. North American cold events following SSW in the presence of lower BKS sea ice

We begin by showing the importance of the SIC in the BKS region for the influence of SSWs on the cold events over North America. Figures 1(a)–(b) compares the SAT and near-surface wind anomalies averaged over days 20–40 following the onset of SSWs, for the winters in which the preceding late autumn SIC over the BKS region is lower and higher than normal, respectively, in observations. The reason we focus on days 20–40 is that the SAT anomaly difference between these two cases is distinct during this period (will be discussed in figures 3 and 4). In contrast to very weak SAT anomalies in the winters with higher BKS SIC (HiSIC; figure 1(b)), a large decrease in SAT is found over Canada and central and midwestern US, 20–40 d after the onset of SSWs in the winters with lower BKS SIC (LoSIC; figure 1(a)). These SAT anomalies are significantly different between the two sea ice conditions (figure 1(c)). These surface cold anomalies in lower BKS SIC winters are consistent with cold air advection by anomalous northeasterlies blowing from the Arctic region to North America. The results remain robust if the lower and higher SIC winters are defined with 2–9 year bandpass filtered BKS SIC time series that focus on the interannual variability and with the removal of the last 10 years in which the sea ice rapidly declines (figures S1–S2).

The identification of causality among the BKS sea ice, SSWs and North American cold events in observations is challenging, since midlatitude circulation anomalies could also possibly contribute to changes in BKS sea ice [11]. Thus, we have used an AGCM with a well-resolved stratosphere, and conducted numerical model experiments with and without prescribed BKS sea ice reduction to demonstrate the critical role of BKS sea ice conditions. The model results support the observed connection between the SSWs and North American SATa (figures 1(d)–(f)). Comparing the model results with and without lower BKS sea ice (referred to as BKSIC run and Ctrl run), an enhancement of cold anomalies is found over North America in the former.

During the latest 2019 cold event, the record-breaking cold temperature over the midwestern U.S. was observed on Jan. 30–31, 2019 [40], lagging the SSW that occurred on 30 December 2018 by about one month. The preceding early winter BKS SIC anomaly was −14%, the fifth lowest value in the past 40 years (figure S1(a)). As shown in figure 1(g), the North American SAT anomaly pattern during days 20–40 in the 2019 case highly resembles that of the LoSIC composite as shown in figure 1(a) except that the 2019 event exhibits a larger amplitude than the composite likely from the internal variability of the atmosphere.

In addition, the impact of BKS sea ice reduction on cold events is also reflected in the number of extreme cold days after SSWs (figure 2). Here we define an extreme cold day as a day during which the SAT is at least 1 standard deviation (σ) below its climatology. Compared to 2–3 extreme cold days in the higher sea ice cases (figure 2(b)), more than five extreme cold days occur across the most part of Canada and Midwest U.S. in days 20–40 following the SSWs in the lower BKS sea ice cases (figure 2(a)). The increase of North American cold days is statistically significant (figure 2(c)) and also holds for thresholds of $1.5\sigma$ and $2\sigma$ (not shown). A similar increase of extreme cold days can be found in model simulations (figures 2(d)–(f)) with consistent spatial patterns, although the increase is smaller.

Figures 3(a)–(b) displays the PDF of area averaged daily SAT anomaly and its temporal evolution after the onset of SSWs under different sea ice conditions. In the winters with lower BKS sea ice, there is a shift ($P < 0.01$) in the PDF toward colder SAT during days 10–50 after SSWs (solid blue) as compared to that for all winter days (dashed blue) and to that for higher BKS sea ice SSWs (solid red). As the largest surface cooling over North America takes place 20–40 d after the onset of SSWs and its differences to that in higher sea ice conditions are significant (figure 3(b)), it is promising that SSWs combined with BKS sea ice conditions can be used as a predictor for North American cold events at the subseasonal timescale. It is worthy to note that the aim of this study is to explore the potential subseasonal predictability of BKS sea ice on SSW related weather extremes and thus only the SATa during the weeks following SSW are discussed here, and the changes in these SATa may have little impact on the whole winter SATa distribution over North America (contrast the dashed red and blue curves in figure 3(a)). Although the modeled PDF shapes are slightly different from the observations due to the distinct sample size, a shift of PDF toward the colder flank of the SATa after SSWs in model experiments is in agreement with observations (figures 3(c) and (d)). While the magnitude of surface cooling is slightly weaker in the model experiments than that in observations, the broad consistency in the spatial patterns and timing of the SAT

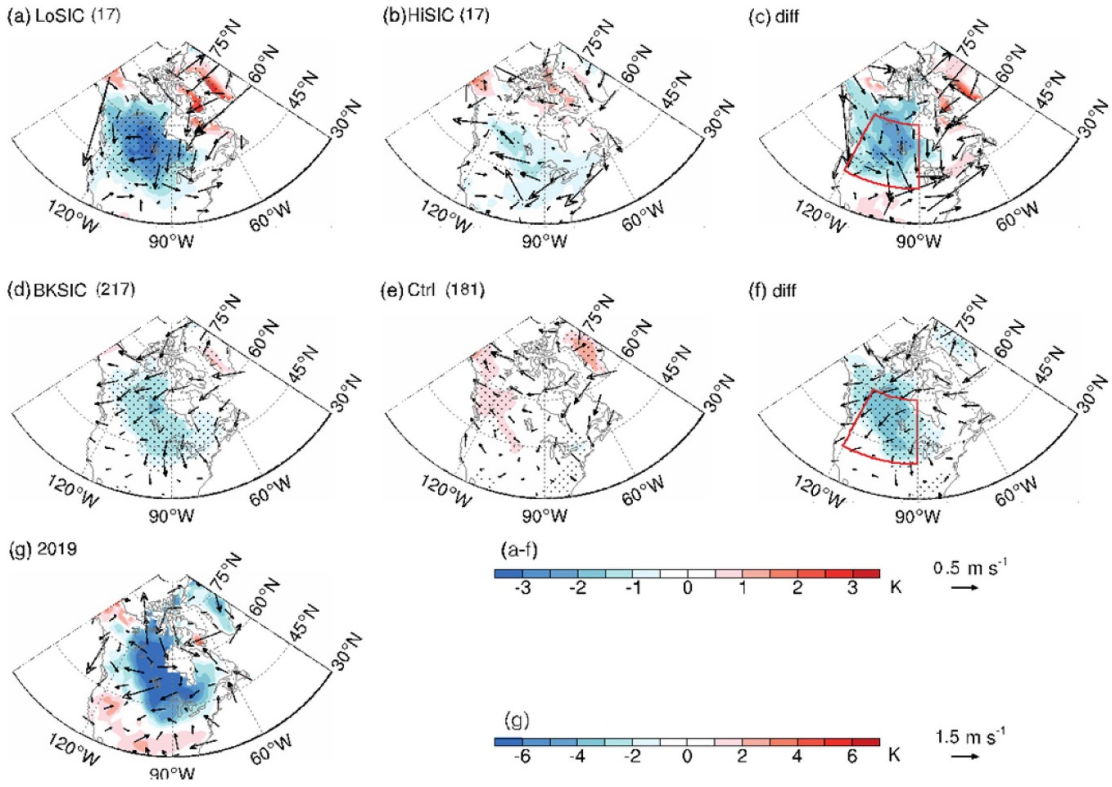


**Figure 1.** Surface air temperature anomalies following SSWs with different BKS sea ice conditions. (a–c) Surface air temperature (SAT, color shading) and surface wind (vector) anomalies during days 20–40 in lower (LoSIC), higher (HiSIC) BKS sea ice conditions and their differences in observations. (d–f) Same as (a–c) but for those in the BKSIC and Ctrl experiments and their differences. Stippling denotes regions that are different from zero in a, b, d, e or from each other in c, f at the 95% confidence level for SAT anomalies. (g) The 2019 case anomalies during Jan.19–Feb.7, 2019. The samples sizes for the composites analysis in (a, b, d, e) are shown at the upleft corner.

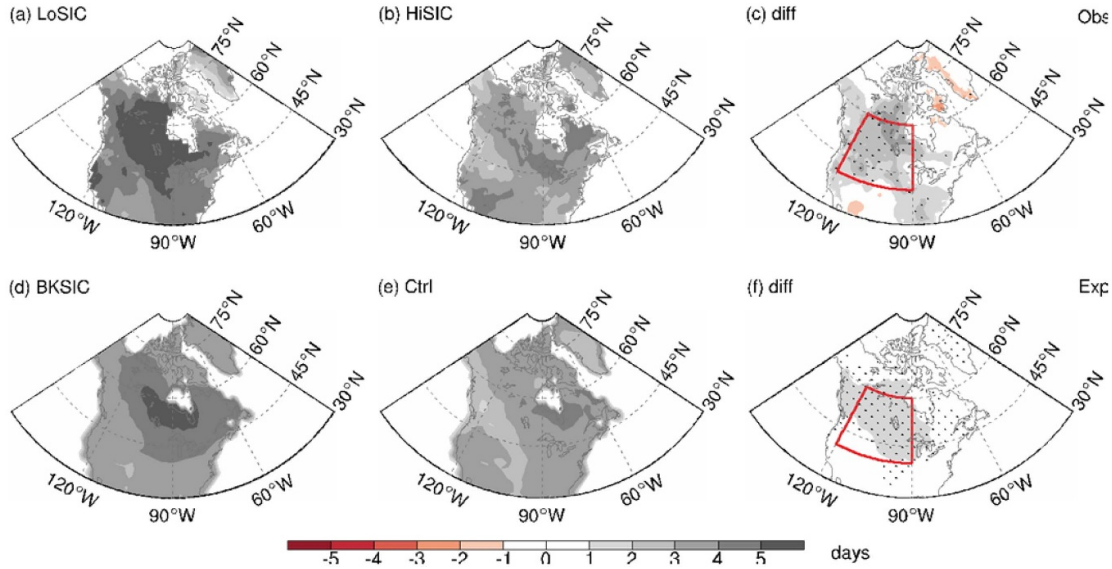


**Figure 2.** Numbers of cold days following SSWs and their changes. (a–c) Extreme cold day numbers during days 20–40 in lower (LoSIC), higher (HiSIC) BKS sea ice conditions and their differences in observations. (d–f) Same as (a–c) but for those in the BKSIC and Ctrl experiments and their differences. Stippling in (c, f) denotes the regions that are statistically significantly different from each other at the 95% confidence level.

anomalies between model simulations and observations confirms the critical role of the lower BKS sea ice on the SSW-induced cold events over North America.

Moreover, the relative contribution of stratospheric versus tropospheric processes to anomalous surface cooling is assessed by supplementary

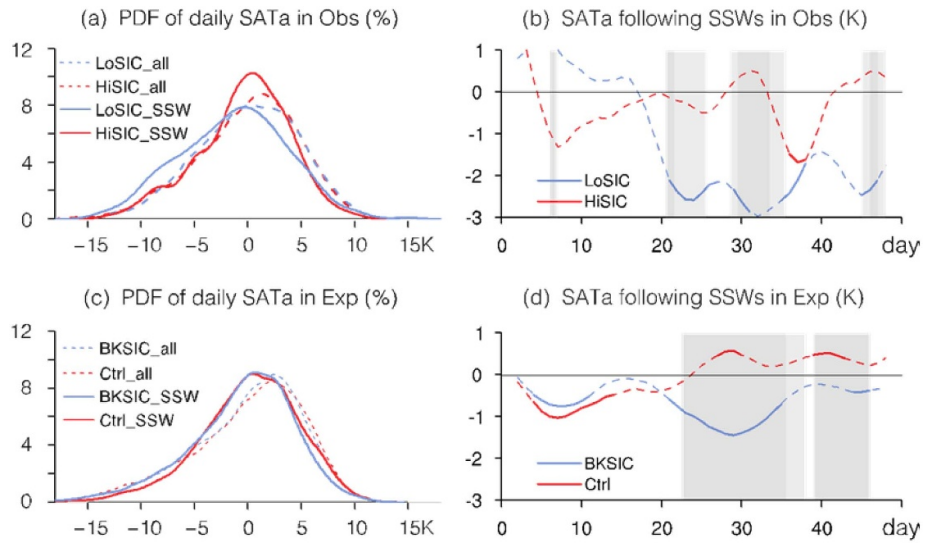


**Figure 3.** Probability Distribution Function (PDF) of North American daily SAT anomaly and its time evolution following SSWs. (a, c) PDF of daily SAT anomaly in all days in low sea ice winters (LoSIC_all/BKSIC_all, dashed blue line), all days in high sea ice winters (HiSIC_all/Ctrl_all, dashed red line) and during days 10–50 following SSWs in low sea ice winters (LoSIC_SSW/BKSIC_SSW, solid blue line) and high sea ice winters (HiSIC_SSW/Ctrl_SSW, solid red line) in observations (a) and experiments (c). (b, d) Time evolution of NA SATa in observations and experiments following SSW. The time series is the area-weighted average over (40°–60°N, 90°–120°W), the red box in figures 1 and 2. The time series in blue and red show the evolution of SAT anomalies in lower and higher SIC conditions, respectively. The solid segments in (b, d) denote the SAT anomaly that is significant to their climatologies at the 95% confidence level. The deep (light) gray bars in (b, d) show the differences between two time series of SAT anomalies are significant at 95% (90%) confidence level.

experiments, in which the stratospheric and tropospheric pathways are separated by isolating the circulation response in the stratosphere and troposphere, respectively (see details in SM). The stratospheric pathway experiment, in which no sea ice reduction is prescribed but the stratospheric circulation is nudged to that of the lower sea ice experiment (BKSIC run), also shows significant anomalous surface cooling over North America following the onset of SSWs (figure S3(a)). In contrast, the SATa following SSWs is nearly absent and even a warm anomaly over the western Canada is found in the tropospheric pathway experiment, in which the same sea ice reduction is imposed in the model but the stratospheric processes are suppressed by nudging the stratospheric circulation to that of the control simulation (figure S3(b)). This further confirms that the cold anomalies identified in figure 1 are largely the downward influence of SSWs in the presence of lower BKS sea ice rather than the direct tropospheric circulation response to sea ice anomaly.

### 3.2. SSWs influence North America by the regional effect of planetary waves

How can SSWs influence the SAT over North America with a lead time of about one month? The Northern Annular Mode (NAM) index, commonly used to explain the downward influence of SSWs, shows that the downward propagation from the stratosphere to the surface is enhanced under the lower BKS sea ice condition (figure S4). However, it is hard to employ the downward propagation of anomalous zonal mean zonal flow to explain the regional temperature signals over North America. Thus, an alternative explanation is provided here from the perspective of the regional effect of planetary waves.

We first present the mid-tropospheric circulation pattern following SSW events associated with lower BKS SIC (figure 4). In the mid-troposphere, there is a ridge over the Gulf of Alaska in observations in winter climatology (blue contours in figure 4). Under lower SIC conditions in observations, an extensive positive 500 hPa geopotential height (Z) anomaly is found over the Bering Sea to Gulf of Alaska (BSGA) (150°E–150°W), manifesting a reinforced ridge in this case (figure 4(a)). The resulting enhanced northwesterly wind to the east of the ridge brings more cold air from the Arctic to North America. With the intensified southward sinking of cold air mass, near-surface northeasterlies and associated cold air advection inland are developed downstream of the intensified mid-level BSGA ridge (figure 1). On the contrary, SSWs in higher BKS sea ice conditions are accompanied by mostly negative Z anomalies over the BSGA (figure 4(b)). The most pronounced feature in the differences between the two composites is a high-pressure anomaly over the BSGA, favoring a downstream northerly anomaly and cold air outbreaks (figure 4(c)). Similar results in the mid-tropospheric circulation are simulated in the AGCM experiments with and without BKS sea ice loss, especially for the BSGA ridge anomaly, despite that the Z anomalies are only found over the BSGA while the observed Z anomalies occupy the whole northern

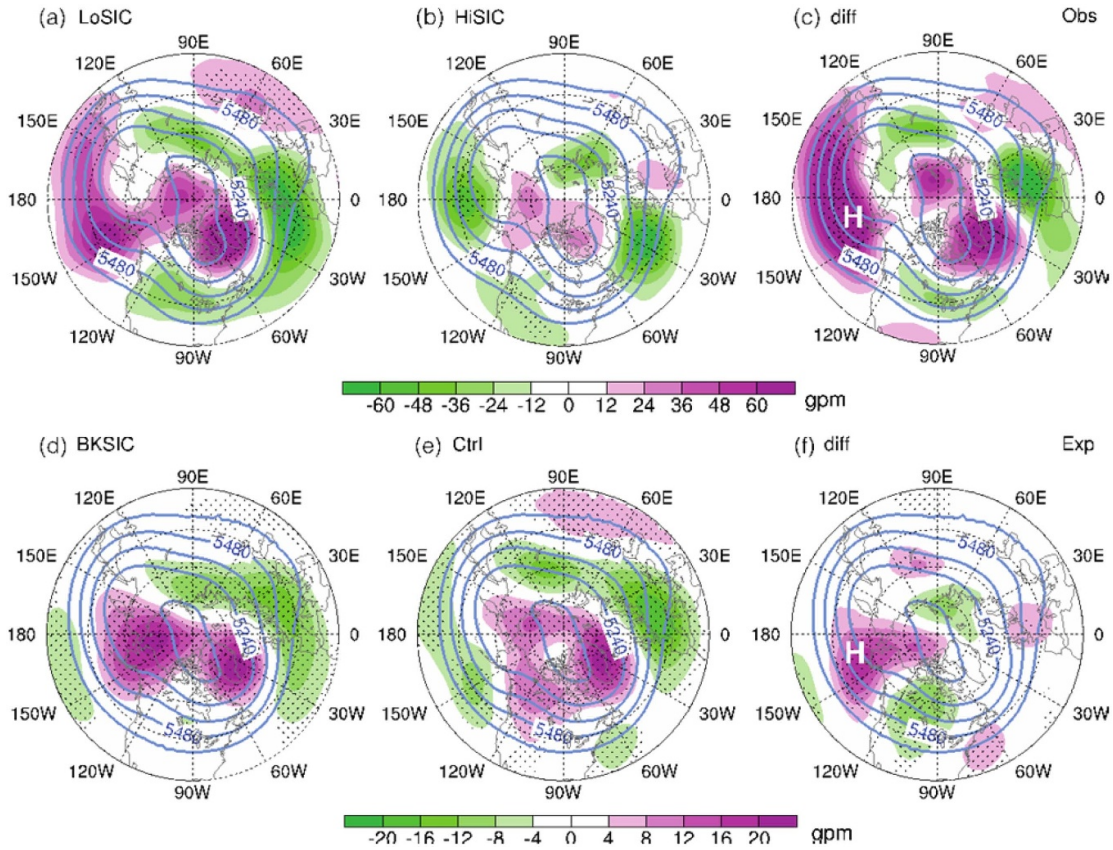


**Figure 4.** Mid-tropospheric circulation anomalies following SSWs under different sea ice conditions. (a–b) Geopotential height anomalies (Z, color shading) at 500 hPa during day 20–40 following SSWs in low and high sea ice winters in observations. (c) Difference of Z anomaly between (a) and (b). The blue contours present the Z winter climatology with 160 gpm interval. (d–f) Same as (a–c) but for the BKSIC and Ctrl runs and their differences. The contours in (d–f) are the average of the winter Z climatologies in Ctrl and BKS runs. Stippling denotes regions that are different from zero in a, b, d, e or from each other in c, f at the 95% confidence level for Z anomalies. The letter 'H' in (c, f) marks a high pressure (ridge) anomaly over the Bering Sea-Gulf of Alaska under the low sea ice condition that is conducive to North America cold temperature anomalies in figure 1

North Pacific (figures 4(d)–(f)). Thus, the deepened mid-tropospheric BSGA ridge is the key to the anomalous surface cooling in response to SSWs under lower BKS SIC.

The mid-tropospheric BSGA ridge anomaly is associated with the planetary WAF that first displays an enhanced upward propagation into the stratosphere around the SSW onset and subsequently turns eastward (i.e. suppressed upward propagating waves) in the troposphere over the North Pacific (120°E–120°W) and converges over 180°–150°W favoring the ridging over the BSGA (figure S5), which is consistent with the planetary wave characteristics following stratospheric warming events in previous studies [41, 42] (see more discussion in SM). Accordingly, a coherent vertical wave structure from the mid-troposphere to the stratosphere can be found in Z differences between low and high sea ice conditions over the North Pacific to North America (120°E–60°W) (figures S6(a) and (b)). Moreover, the daily evolution of the Z anomaly averaged over the BSGA region, coinciding with a planetary wave-2 ridge anomaly that starts descending from the lower stratosphere (50 hPa) around day 16 to the mid-troposphere around day 24 (figures S6(c) and (d)), shows a persistent ridge anomaly in the troposphere starting from approximately day 24 after the onset of SSW events, confirming the downward coupling timescale revealed in figure S4. The downward descent of the wave-2 ridge anomaly from the lower stratosphere demonstrates the key role of the planetary wave-2 component in the establishment of the mid-tropospheric BSGA ridge and associated North American surface cooling to SSWs.

These lower stratospheric anomalies arise from the slow recovery of the stratospheric polar vortex after SSW and associated upward propagating planetary wave activity. Figure S7 depicts the evolution of the stratospheric polar vortex anomalies and associated wave-2 component in the lower stratosphere. Figure 5 is the same but for the average of days 20 to 40. It can be seen that, under low BKS SIC conditions, the stratospheric polar vortex is persistently distorted with two ridges of wave-2 anchored over the Eastern Siberia and Greenland and two troughs over Alaska and Ural Mountain for about 40 d after the onset of SSWs, indicating a persistent stretching

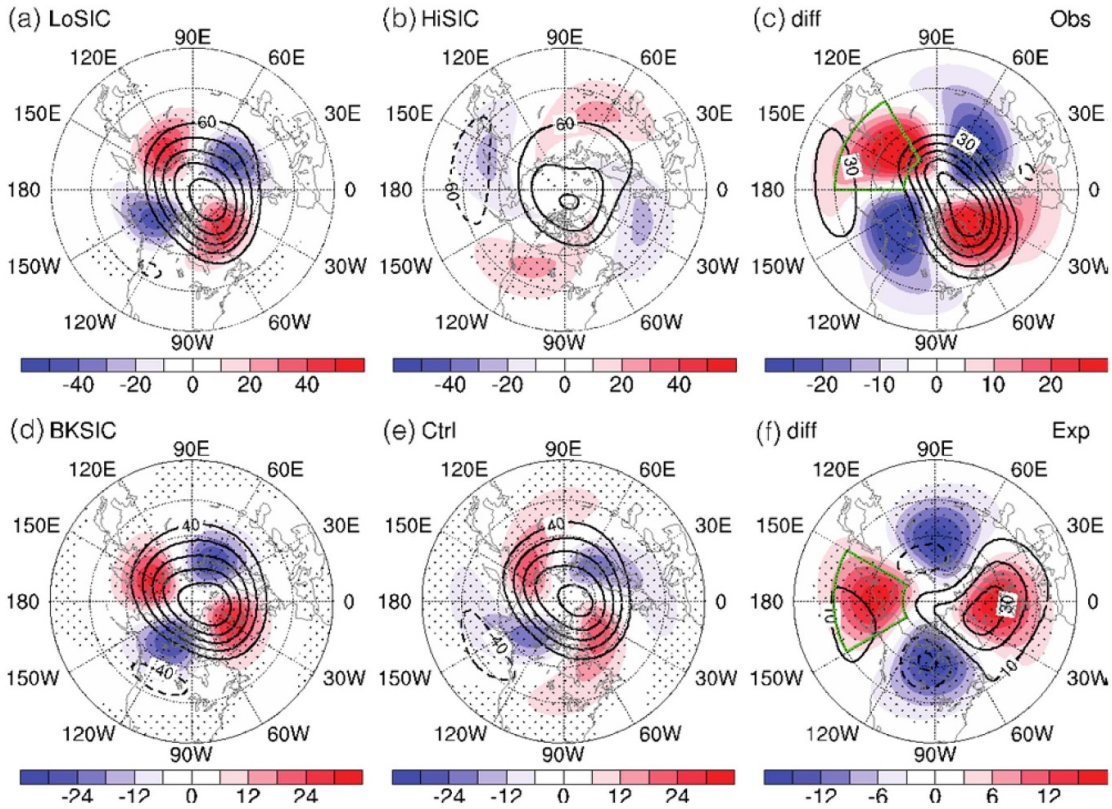


**Figure 5.** Stratospheric circulation anomalies following SSWs under different sea ice conditions. (a–c) 70-hPa Z (contour) and wave-2 (color) anomalies averaged over day 20 to day 40 following SSWs during LoSIC and HiSIC winters and their differences in observations. (d–f) Same as (a–c) but for the BKSIC and Ctrl runs and their differences. The contour intervals are 60gpm in (a, b), 30gpm in (c), 40gpm in (d, e) and 10gpm in (f). Stippling denotes regions that are different from zero in a, b, d, e or from each other in c, f at the 95% confidence level for Z anomalies. Green boxes in (c, f) highlight the differences of wave-2 ridge anomalies in observation (45°–75°N, 120°–180°E) and model experiments (45°–75°N, 150°E — 210°W) linked to the mid-tropospheric Bering Sea and Gulf of Alaska ridge. It should be noted that there is a slight shift of the wave structure and thus the position of wave-2 anomalies in model experiments as compared to that in observations.

of the polar vortex, and this is true in both observations and experiments (figures 5(a), (d) and S7(a), (d)). However, this is not the case under high BKS SIC conditions (figures 5(b), (e) and S7(b), (e)), instead the wave-2 anomaly pattern shifts in longitude and decays with time. Therefore, following the SSW in low BKS SIC winters, the persistent ridge of wave-2 anomaly over eastern Siberia extends from the stratosphere to the troposphere, enhancing the mid-tropospheric ridge over BSGA that favors downstream cold air outbreaks. While the maximal wave-2 differences between the low and high BKS SIC conditions in AGCM are slightly shifted to the east by about 30 degrees compared to observations (figures 5(c) and (f)), the basic features of the wave-2 vertical structures are similar (figure S6).

Given the small sample size of SSWs in observations (17/17), we further demonstrate the robustness of observational results in the view of probability distribution based on a stochastic resampling of 17 events from the abundant samples in model simulations (217/181). Figure 6 shows the 2-D kernel density estimate for North American SAT anomaly and stratospheric wave-2 anomaly over the northern North Pacific (green box in figures 5(c) and (f)) following the SSWs. The wide range of probability density indicates that the mean of 17 random samples could have a large spread due to the internal variability of the atmosphere. However, it is clear that there are significant changes in the probability distribution between lower and higher BKS SIC. The density distribution shifts to an enhancement of the stratospheric wave-2 ridge and colder North American SAT under the lower BKS sea ice conditions (figure 6(a)). This shift between the two resampling groups is similar to that of the means of two observational groups. Similar conclusions are also found in the extreme cold days, with more cold days following SSWs due to the enhancement of the persistent wave-2 ridge under lower BKS sea ice condition (figure 6(b)).

### 3.3. Role of lower BKS sea ice

A remaining question is how the BKS sea ice reduction changes the stratospheric polar vortex geometry during SSWs and thereafter its downward influence. It has been recognized that the sea ice decline over the BKS region can effectively enhance the upward planetary-scale wave propagation into the stratosphere via linear constructive interference and thereby modify the stratospheric polar

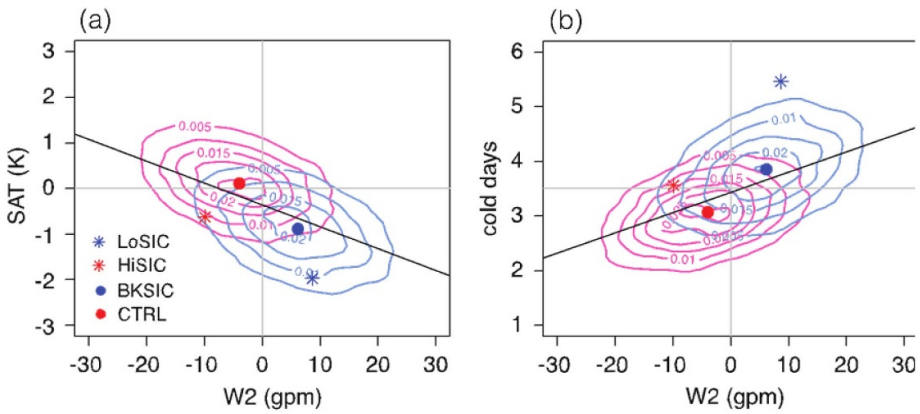


**Figure 6.** Bivariate density of North American SAT anomaly and wave-2 ridge anomaly in the stratosphere. (a) Two-dimensional (2D) kernel density estimates of North Pacific 70hPa Z wave-2 anomalies and North America SAT anomalies during days 20–40, based on 10 000 times bootstrap resampling for the mean of 17/17 samples (the sample sizes in LoSIC and HiSIC) from the simulated 217/181 events in BKSIC and Ctrl runs. The blue (pink) contours denote the 2-D density in lower (higher) SIC condition. The stars denote the mean values in LoSIC and HiSIC in observation. The solid dots denote the means in BKSIC run and Ctrl runs. The black line is the linear fitting based on the total resampling of two groups. (b) Same as (a) but for the 2-D density estimate of wave-2 anomalies and North America extreme cold day numbers during days 20 to 40. See more details of the resampling for the 2-D kernel density estimate in Method. The ridge anomalies are calculated as the area-weighted average in the green boxes shown in figures 5(c) and (f) for observation and model experiment, respectively.

vortex [43, 44]. Heat flux ($v'T'$) activity is generally employed to measure the wave activity during SSWs. Figure S8 shows the anomalies of 100hPa heat flux by wave-1 and wave-2 averaged during days −8 to −1 prior to SSW onset, the embryonic stage of the SSW during which upward coupling is prevailing. For the wave-1 heat flux component prior to SSW onset, a similar amplified heat flux is found in both observations and AGCM experiments regardless of BKS sea ice conditions (figures S8(a)–(f)).

The differences are, however, notable in the wave-2 heat flux anomalies. Under lower BKS sea ice conditions, an enhancement of wave-2 heat flux can be seen at high latitudes (figures S8(g), (j)). In comparison, in the absence of BKS sea ice reduction, the wave-2 heat flux anomalies are weaker (figures S8(h), (i), (k) and (l)). The significantly intensified wave-2 heat flux anomalies with lower BKS sea ice highlight the important role of wave-2 component, favoring polar vortex stretching, in the evolution of the polar vortex during SSW, which is also consistent with previous section and previous finding that the preceding enhanced wave-2 activity from the troposphere favors the split SSWs (the extreme case of polar vortex stretching) [45–47].

## 4. Conclusions

In summary, we demonstrate in both observations and model experiments that the likelihood that SSWs lead to North American cold events is increasing in the presence of lower BKS sea ice. This linkage between the early winter sea ice condition and SSWs as a subseasonal precursor of North American cold events has not been established before. The timing and structure of the record-breaking cold air outbreak in late January 2019 and the preceding SSW share many similarities with our composite analysis, even though an individual event is known to be strongly affected by the internal variability of the atmosphere. We find that in response to lower BKS SIC, the enhanced upward wave-2 propagation from the troposphere into the stratosphere stretches the stratospheric polar vortex pattern during SSWs and favors a persistent ridge anomaly over the Eastern Siberia in the lower stratosphere following SSWs. The ridge anomaly in the wave-2 pattern migrates downward and causes a mid-tropospheric ridge anomaly over the Bering Sea-Gulf of Alaska region and associated colder North America, which persists for several weeks or so after the SSW onset. We stress that this dynamical pathway is key to the regional effects of planetary-scale waves. This mechanism is distinct from the previous studies that emphasized the conventional downward influence of SSWs based on a zonal mean flow-eddy feedback framework [17, 18, 20, 25], and shares similarities with the planetary wave characteristics associated with North American cold events in recent studies [41, 42].

In spite of a weakening of the seasonal mean stratospheric polar vortex as a result of lower BKS sea ice [30], we find no significant change in the frequency of SSW events in observations, despite limited samples, but a slight increase in AGCM experiments based on abundant samples (figure S9). The aforementioned mechanism of the regional effect of planetary waves may also be associated with other stratospheric processes such as the Quasi-Biennial Oscillation, that modulates the residual circulation, subtropical wave dissipation [48] and wave coupling pattern [49]. Although the splitting SSWs are usually

modulated by strong wave-2 activity, the wave-2 pattern prior to North American cold events is not necessarily linked to the types of SSWs (i.e. displacement or splitting; see table S1). In these displacement SSWs in LoSIC winters, the wave-2 disturbances are not strong enough to split the polar vortex (not shown) but sufficient to cause a BSGA ridge anomaly and therefore cooling over North America following the SSWs. Although recent studies suggested that the direct impact of Arctic warming on midlatitude winter mean temperature may be limited [12], our analysis demonstrates that the combined knowledge of late autumn Arctic sea ice conditions and stratospheric circulation patterns will help improve predictability over North America on the subseasonal timescale.

## Acknowledgments

We thank Dr Isla R Simpson and two reviewers for their helpful suggestions. We would like to acknowledge high-performance computing support from Cheyenne (doi:10.5065/D6RX99HX) provided by CISL/NCAR, sponsored by the NSF. PZ and GC were funded by the NSF (AGS-1742178 and AGS-1832842). PZ and YW were funded by the NSF (AGS-1406962). YW also acknowledges the support from the Lamont Center for Climate and Life Fellowship. YY was funded by NNSFC (41705039). The authors declare that they have no competing interests.

## Data availability statement

The data that support the findings of this study are available upon reasonable request from the authors.

## ORCID iDs

Pengfei Zhang https://orcid.org/0000-0003-3562-9717
Yutian Wu https://orcid.org/0000-0002-4428-6624
Gang Chen https://orcid.org/0000-0003-4934-1909
Yueyue Yu https://orcid.org/0000-0002-1885-3074

## References

[1] Johnson N C, Xie S-P, Kosaka Y and Li X 2018 Increasing occurrence of cold and warm extremes during the recent global warming slowdown *Nat. Commun.* **9** 1724
[2] Cohen J, Pfeiffer K and Francis J A 2018 Warm Arctic episodes linked with increased frequency of extreme winter weather in the United States *Nat. Commun.* **9** 869
[3] Screen 2017 Simulated atmospheric response to regional and pan-arctic sea ice loss *J. Clim.* **30** 3945–62
[4] Overland J, Wood K R and Wang M 2011 Warm Arctic—cold continents: climate impacts of the newly open Arctic Sea *Polar Res.* **30** 15787
[5] Inoue J, Hori M E and Takaya K 2012 The role of barents sea ice in the wintertime cyclone track and emergence of a warm-Arctic cold-Siberian anomaly *J. Clim.* **25** 2561–8
[6] Kug J-S, Jeong J-H, Jang Y-S, Kim B-M, Folland C K, Min S-K and Son S-W 2015 Two distinct influences of Arctic warming on cold winters over North America and East Asia *Nat. Geosci.* **8** 759–62
[7] Mori M, Kosaka Y, Watanabe M, Nakamura H and Kimoto M 2019 A reconciled estimate of the influence of Arctic sea-ice loss on recent Eurasian cooling *Nat. Clim. Change* **9** 123–9
[8] Barnes E A 2013 Revisiting the evidence linking Arctic amplification to extreme weather in midlatitudes *Geophys. Res. Lett.* **40** 4734–9
[9] McCusker K E, Fyfe J C and Sigmond M 2016 Twenty-five winters of unexpected Eurasian cooling unlikely due to Arctic sea-ice loss *Nat. Geosci.* **9** 838–42
[10] Sun L, Perlwitz J and Hoerling M 2016 What caused the recent 'Warm Arctic, Cold Continents' trend pattern in winter temperatures? *Geophys. Res. Lett.* **43** 5345–52
[11] Peings Y 2019 Ural blocking as a driver of early-winter stratospheric warmings *Geophys. Res. Lett.* **46** 5460–8
[12] Blackport R, Screen J A, van der Wiel K and Bintanja R 2019 Minimal influence of reduced Arctic sea ice on coincident cold winters in mid-latitudes *Nat. Clim. Change* **9** 697–704
[13] Screen J A, Deser C, Smith D M, Zhang X, Blackport R, Kushner P J, Oudar T, McCusker K E and Sun L 2018 Consistency and discrepancy in the atmospheric response to Arctic sea-ice loss across climate models *Nat. Geosci.* **11** 2073–6
[14] Cohen J *et al* 2020 Divergent consensuses on Arctic amplification influence on midlatitude severe winter weather *Nat. Clim. Change* **10** 20–29
[15] Acosta Navarro J C *et al* 2020 Link between autumnal arctic sea ice and northern hemisphere winter forecast skill *Geophys. Res. Lett.* **47** e2019GL086753
[16] Mohammadi-Aragh M, Goessling H F, Losch M, Hutter N and Jung T 2018 Predictability of Arctic sea ice on weather time scales *Sci. Rep.* **8** 6514
[17] Polvani L M and Waugh D W 2004 Upward wave activity flux as a precursor to extreme stratospheric events and subsequent anomalous surface weather regimes *J. Clim.* **17** 3548–54
[18] Baldwin M P and Dunkerton T J 2001 Stratospheric harbingers of anomalous weather regimes *Science* **294** 581–4
[19] Mitchell D M, Gray L J, Anstey J, Baldwin M P and Charlton-Perez A J 2013 The influence of stratospheric vortex displacements and splits on surface climate *J. Clim.* **26** 2668–82
[20] Hitchcock P and Simpson I R 2014 The downward influence of stratospheric sudden warmings *J. Atmos. Sci.* **71** 3856–76
[21] Thompson D W J, Baldwin M P and Wallace J M 2002 Stratospheric connection to northern hemisphere wintertime weather: implications for prediction *J. Clim.* **15** 1421–8
[22] Kidston J, Scaife A A, Hardiman S C, Mitchell D M, Butchart N, Baldwin M P and Gray L J 2015 Stratospheric influence on tropospheric jet streams, storm tracks and surface weather *Nat. Geosci.* **8** 433–40
[23] Lehtonen I and Karpechko A Y 2016 Observed and modeled tropospheric cold anomalies associated with sudden stratospheric warmings *J. Geophys. Res.* **121** 1591–610
[24] NOAA National Weather Service 2019 Late January 2019 Extreme Cold Summary (https://www.weather.gov/fgf/2019_01_29-31_ExtremeCold) (Retrieved 31 May 2019)
[25] Sun L, Robinson W A and Chen G 2012 The predictability of stratospheric warming events: more from the troposphere or the stratosphere? *J. Atmos. Sci.* **69** 768–83
[26] Yoden S, Ishioka K, Durran D, Enomoto T, Hayashi -Y-Y, Miyoshi T and Yamada M 2014 Theoretical aspects of variability and predictability in weather and climate systems *Bull. Am. Meteorol. Soc.* **95** 1101–4

[27] Tripathi O P et al 2015 The predictability of the extratropical stratosphere on monthly time-scales and its impact on the skill of tropospheric forecasts Q. J. R. Meteorol. Soc. 141 987–1003
[28] Noguchi S, Kuroda Y, Mukougawa H, Mizuta R and Kobayashi C 2020 Impact of satellite observations on forecasting sudden stratospheric warmings Geophys. Res. Lett. n/a e2019GL086233
[29] Nakamura T, Yamazaki K, Iwamoto K, Honda M, Miyoshi Y, Ogawa Y, Tomikawa Y and Ukita J 2016 The stratospheric pathway for Arctic impacts on midlatitude climate Geophys. Res. Lett. 43 3494–501
[30] Zhang P, Wu Y, Simpson I R, Smith K L, Zhang X, De B and Callaghan P 2018 A stratospheric pathway linking a colder Siberia to Barents-Kara Sea sea ice loss Sci. Adv. 4 eaat6025
[31] Siew P Y F, Li C, Sobolowski S P and King M P 2020 Intermittency of Arctic–mid-latitude teleconnections: stratospheric pathway between autumn sea ice and the winter North Atlantic Oscillation Weather Clim. Dyn. 1 261–75
[32] Dee D P et al 2011 The ERA-Interim reanalysis: configuration and performance of the data assimilation system Q. J. R. Meteorol. Soc. 137 553–97
[33] Cavalieri D J, Parkinson C L, Gloersen P and Zwally H J 1996 Sea Ice Concentrations from Nimbus-7 SMMR and DMSP SSM/I-SSMIS Passive Microwave Data, Version 1 Ed (Boulder, Colorado USA: National Snow and Ice Data Center) (https://doi.org/10.5067/8GQ8LZQVL0VL)
[34] Koenigk T, Caian M, Nikulin G and Schimanke S 2016 Regional Arctic sea ice variations as predictor for winter climate conditions Clim. Dyn. 46 317–37
[35] Butler A H, Seidel D J, Hardiman S C, Butchart N, Birner T and Match A 2015 Defining sudden stratospheric warmings Bull. Am. Meteorol. Soc. 96 1913–28
[36] Smith K L, Neely R R, Marsh D R and Polvani L M 2014 The specified chemistry whole atmosphere community climate model (SC-WACCM) J. Adv. Model. Earth Syst. 6 883–901
[37] Mori M, Watanabe M, Shiogama H, Inoue J and Kimoto M 2014 Robust Arctic sea-ice influence on the frequent Eurasian cold winters in past decades Nat. Geosci. 7 869–73
[38] Rosenblum E and Eisenman I 2017 Sea ice trends in climate models only accurate in runs with biased global warming J. Clim. 30 6265–78
[39] Li D, Zhang R and Knutson T R 2017 On the discrepancy between observed and CMIP5 multi-model simulated Barents Sea winter sea ice decline Nat. Commun. 8 14991
[40] NOAA National Centers for Environmental Information 2019 State of the Climate: National Climate Report for January 2019 (https://www.ncdc.noaa.gov/sotc/national/201901)
[41] Kodera K, Mukougawa H, Maury P, Ueda M and Claud C 2016 Absorbing and reflecting sudden stratospheric warming events and their relationship with tropospheric circulation J. Geophys. Res. 121 80–94
[42] Kretschmer M, Cohen J, Matthias V, Runge J and Coumou D 2018 The different stratospheric influence on cold-extremes in Eurasia and North America Npj Clim. Atmos. Sci. 1 44
[43] Kim B-M, Son S-W, Min S-K, Jeong J-H, Kim S-J, Zhang X, Shim T and Yoon J-H 2014 Weakening of the stratospheric polar vortex by Arctic sea-ice loss Nat. Commun. 5 4646
[44] Hoshi K, Ukita J, Honda M, Iwamoto K, Nakamura T, Yamazaki K, Dethloff K, Jaiser R and Handorf D 2017 Poleward eddy heat flux anomalies associated with recent Arctic sea ice loss Geophys. Res. Lett. 44 446–54
[45] Martius O, Polvani L M and Davies H C 2009 Blocking precursors to stratospheric sudden warming events Geophys. Res. Lett. 36 L14806
[46] Cohen J and Jones J 2011 Tropospheric precursors and stratospheric warmings J. Clim. 24 6562–72
[47] Sheshadri A, Plumb R A and Gerber E P 2015 Seasonal variability of the polar stratospheric vortex in an idealized AGCM with varying tropospheric wave forcing J. Atmos. Sci. 72 2248–66
[48] Gómez-Escolar M, Calvo N, Barriopedro D and Fueglistaler S 2014 Tropical response to stratospheric sudden warmings and its modulation by the QBO J. Geophys. Res. 119 7382–95
[49] Labe Z, Peings Y and Magnusdottir G 2019 The effect of QBO phase on the atmospheric response to projected Arctic sea-ice loss in early winter Geophys. Res. Lett. 46 7663–71